# Structure of Silica Gel Si-60 and Pyrocarbon/Silica Gel Adsorbents Thermally and Hydrothermally Treated

V. M. Gun'ko,*,† R. Leboda,‡ J. Skubiszewska-Zięba,‡ V. V. Turov,† and P. Kowalczyk§

*Institute of Surface Chemistry, 17 General Naumov Street, 03164 Kiev, Ukraine, Department of Chemical Physics, Maria Curie-Sklodowska University, 20-031 Lublin, Poland, and Military Institute of Chemistry and Radiometry, 00-910 Warsaw, Poland*

*Received July 31, 2000. In Final Form: November 30, 2000*

Characteristics of porous structure of silica gel Si-60 (pristine and covered by different amounts of pyrocarbon prepared by pyrolysis of acenaphthene, acetylacetone, and glucose, then heated at 500 °C in air or hydrothermally treated (HTT) at 150 or 200 °C, and also heated at 500 °C) were analyzed by using TEM, $^1$H NMR, and adsorption−desorption of nitrogen at 77.35 K. The structural parameters were estimated by the direct minimization method or the overall isotherm approximation with a regularization procedure. Pyrolysis of different organics on Si-60 is accompanied by marked changes in the pore structure depending on the nature of precursors. Hydrothermal treatment of silica gel and carbosils at 150−200 °C for 6 h results in a strong modification of both pores and outer surfaces of silica gel particles in contrast to heating of pristine Si-60 or carbosils (after HTT) at 500 °C in air for 24 h. Computations of the distributions of the pore size and nitrogen adsorption energy, as well as $^1$H NMR spectra of the interfacial water, reveal an increase in the adsorbent nonuniformity due to hydrothermal treatment, but heating of silica gel and pyrocarbon/silica in air gives the opposite result.

## Introduction

Pyrocarbon/silicas (carbosils) can be appropriate as adsorbents utilized in different media due to their ability to interact effectively with polar and nonpolar compounds.[1,2] The characteristics of carbon deposits and adsorbent as a whole can be changed due to variations in pyrolysis conditions, precursor origin, or pretreatment techniques (chemical modification, hydrothermal and thermal treatments).[1−6] It is known[4−8] that both thermal and hydrothermal treatments (HTT) of silica gels change the pore structure, namely, decrease the specific surface area and increase average pore size, depending on the treatment temperature. One can assume that marked structural alterations in the silica matrix can occur during pyrolysis of organics at 500−700 °C, depending on the nature of reactants. It should be noted that the influence of hydrothermal treatment of hybrid carbon/mineral adsorbents on their texture is inadequately investigated, as well as the impact of the origin of carbonized precursors on the structural parameters of hybrid adsorbents differently treated. Therefore, the aim of this work is to study the impact of pyrolysis of different precursors (acenaphthene, acetylacetone, glucose) on the silica gel (Si-60) surfaces and thermal and hydrothermal treatments of carbosils on their structural characteristics in comparison with those for initial, heated, or hydrothermally treated silica gels.

## Experimental Section

**(a) Materials.** Silica gel Si-60 (Merck) was used as the initial material (grain fraction of 0.1−0.2 mm) to prepare pyrocarbon/silica adsorbents (carbosils) with different concentrations of pyrocarbon ($C_C$). For comparison, silica gels Si-40 (Merck) (specific surface area $S_{BET} = 732$ m$^2$/g, total pore volume $V_p = 0.542$ cm$^3$/g, average pore radius $R_p = 1.48$ nm), Si-40-HTT ($T_{HTT} = 150$ °C, $S_{BET} = 309$ m$^2$/g, $V_p = 0.512$ cm$^3$/g, $R_p = 3.31$ nm; or $T_{HTT} = 200$ °C, $S_{BET} = 107$ m$^2$/g, $V_p = 0.497$ cm$^3$/g, $R_p = 9.3$ nm); Si-100 (Merck) ($S_{BET} = 332$ m$^2$/g, $V_p = 1.153$ cm$^3$/g, $R_p = 6.95$ nm), and Si-100-HTT ($T_{HTT} = 200$ °C, $S_{BET} = 49$ m$^2$/g, $V_p = 0.18$ cm$^3$/g, $R_p = 7.7$ nm) were utilized. Silica gel was dried at 200 °C for 24 h then cooled in a desiccator before the pyrolysis of deposited acenaphthene (0.5, 2, or 3 g per 5 g of Si-60 corresponding to AN1, AN2, and AN3 samples at $C_C = 7.0$, 15.8, and 22.7 wt %, respectively) in a stainless steel autoclave (0.3 L) at 500 °C for 6 h. The pyrolysis of acetylacetone adsorbed in the amounts of 0.02, 0.03, and 0.04 M per 5 g of Si-60 gave the series of carbosils AC1, AC2, and AC3 ($C_C = 4$, 9.1, and 14.5 wt %, respectively). The carbonization of glucose (6 g per 10 g of Si-60) gave carbosil GL ($C_C = 16.5$ wt %). After the reaction, all the prepared carbosils were washed in a Soxhlet apparatus with *N*,*N*-dimethylformamide and acetone. Then after removal of substances not bound to the solid surfaces, the samples were dried at 200 °C.

Hydrothermal treatment of adsorbents (labeled HTT) was carried out in the autoclave at 150 or 200 °C for 6 h. Sample (2 g) of silica gel or carbosil was placed in a quartz vessel in the autoclave containing 20 mL of water, which was heated at 150 °C (Si-60, Si-40, GL, AN*i*) or 200 °C (Si-60, Si-40, Si-100, AC*i*) (these conditions ensured saturated water vapor pressure in the autoclave[9]). After the modification, the samples were dried at 200 °C for 6 h. To investigate the pyrolysis impact of different precursors on the silica matrix structure, pyrocarbon was removed on heating at 500 °C for 24 h in air (labeled T). The amounts of

* To whom correspondence should be addressed. Fax: 380 44 4443567. E-mail: vlad-gun@carrier.kiev.ua.
† Institute of Surface Chemistry.
‡ Maria Curie-Sklodowska University.
§ Military Institute of Chemistry and Radiometry.

(1) (a) *Adsorption on New and Modified Inorganic Sorbents*; Dabrowski, A., Tertykh, V. A., Eds.; Elsevier: Amsterdam, 1996. (b) Leboda, R. *Mater. Chem. Phys.* **1992**, *31*, 243; **1993,** *34*, 123.
(2) Leboda, R. *Polish Appl. Chem.* **1988,** *32*, 229.
(3) McDaniel, M. P.; Hottovy, T. D. *J. Colloid Interface Sci.* **1980,** *78*, 31
(4) Leboda, R.; Mendyk, E.; Gierak, A.; Tertykh, V. A. *Colloid. Surf. A* **1995,** *105*, 181.
(5) Leboda, R.; Mendyk, E.; Gierak, A.; Tertykh, V. A. *Colloid. Surf. A* **1995,** *105*, 191.
(6) Leboda, R.; Mendyk, E. *Mater. Chem. Phys.* **1991,** *27*, 189.
(7) *The Surface Properties of Silicas;* Legrand, A. P., Ed.; Wiley: New York, 1998.
(8) Proc. Int. Conf. Silica Sci. Technol. "Silica 98"; Mulhouse: France, Sept 1−4, 1998.
(9) *Physicochemical Hanbook;* WNT: Warsaw, 1974; p 132.

10.1021/la001094t CCC: $20.00 
Published on Web 04/27/2001

**Table 1. Structural Parameters of Initial and Modified Si-60, Thermally Treated (T) at 500 °C and Hydrothermally Treated (HTT) at 150 °C (Si-60, AN, GL) and 200 °C (Si-60, AC)**

| adsorbent | $C_C$, wt % | $S_{BET}$, m²/g | $V_p$, cm³/g | $R_p$, nm | $V_\Sigma$, cm³/g | $S_\alpha$, m²/g | $S_{mes}$, m²/g | $S_{DS}$, m²/g | $V_{DS}$, cm³/g | $x_{DS}$, nm | $\delta_{DS}$, nm |
|---|---|---|---|---|---|---|---|---|---|---|---|
| Si-60 | | 369 | 0.753 | 4.1 | 0.753 | 363 | 363 | 169 | 0.19 | 0.90 | 0.49 |
| Si-60-T | | 362 | 0.747 | 4.1 | 0.750 | 361 | 343 | 154 | 0.02 | 0.99 | 0.21 |
| Si-60-HTT-150 | | 121 | 0.731 | 12.1 | 0.790 | 120 | 151 | 36 | 0.08 | 1.03 | 0.14 |
| Si-60-HTT-150-T | | 122 | 0.738 | 12.1 | 0.800 | 115 | 147 | 33 | 0.07 | 1.06 | 0.19 |
| Si-60-HTT-200 | | 47 | 0.272 | 11.8 | | 40 | 27 | 26 | 0.03 | 0.63 | 0.54 |
| Si-60-HTT-200-T | | 46 | 0.305 | 13.0 | | 45 | 27 | 29 | 0.03 | 0.84 | 0.44 |
| AN1 | 7 | 327 | 0.650 | 4.8 | 0.662 | 309 | 290 | 159 | 0.18 | 0.94 | 0.39 |
| AN1-T | | 365 | 0.736 | 4.0 | 0.750 | 357 | 381 | 151 | 0.20 | 0.10 | 0.38 |
| AN1-HTT | | 189 | 0.613 | 6.5 | 0.674 | 181 | 201 | 106 | 0.13 | 0.86 | 0.66 |
| AN1-HTT-T | | 212 | 0.711 | 6.7 | 0.750 | 203 | 236 | 114 | 0.14 | 0.82 | 0.65 |
| AN2 | 15.8 | 244 | 0.480 | 3.9 | 0.557 | 244 | 312 | 108 | 0.13 | 0.96 | 0.40 |
| AN2-T | | 358 | 0.725 | 4.0 | 0.750 | 362 | 351 | 147 | 0.19 | 0.98 | 0.33 |
| AN2-HTT | | 167 | 0.478 | 5.7 | 0.560 | 150 | 132 | 59 | 0.09 | 0.88 | 0.89 |
| AN2-HTT-T | | 181 | 0.714 | 7.9 | 0.750 | 166 | 253 | 130 | 0.13 | 0.61 | 0.61 |
| AN3 | 22.7 | 233 | 0.453 | 3.9 | 0.448 | 222 | 306 | 116 | 0.15 | 0.98 | 0.52 |
| AN3-T | | 337 | 0.726 | 4.3 | 0.750 | 372 | 361 | 140 | 0.09 | 1.12 | 0.12 |
| AN3-HTT | | 150 | 0.385 | 5.1 | 0.450 | 148 | 117 | 79 | 0.11 | 0.99 | 0.59 |
| AN3-HTT-T | | 173 | 0.698 | 8.0 | 0.750 | 163 | 212 | 95 | 0.10 | 0.88 | 0.38 |
| AC1 | 4 | 339 | 0.717 | 4.2 | 0.700 | 327 | 328 | 159 | 0.18 | 0.93 | 0.41 |
| AC1-T | | 345 | 0.743 | 4.3 | 0.750 | 365 | | | 0.19 | 1.03 | |
| AC1-HTT | | 68 | 0.634 | 19.5 | 0.735 | 64 | 63 | 13 | 0.03 | 1.11 | 0.23 |
| AC1-HTT-T | | 60 | 0.709 | 23.5 | 0.780 | 59 | 68 | 28 | 0.04 | 1.03 | 0.45 |
| AC2 | 9.1 | 296 | 0.606 | 4.1 | 0.670 | 287 | 290 | 154 | 0.18 | 0.94 | 0.44 |
| AC2-T | | 340 | 0.730 | 4.3 | 0.750 | 350 | 321 | 187 | 0.18 | 0.97 | 0.53 |
| AC2-HTT | | 90 | 0.648 | 14.5 | 0.700 | 83 | 63 | 66 | 0.05 | 0.78 | 0.28 |
| AC2-HTT-T | | 85 | 0.704 | 16.6 | 0.780 | 77 | 78 | 13 | 0.04 | 1.16 | 0.26 |
| AC3 | 14.5 | 275 | 0.566 | 4.1 | 0.610 | 269 | 274 | 100 | 0.19 | 1.13 | 0.40 |
| AC3-T | | 327 | 0.728 | 4.5 | 0.750 | 326 | | 108 | 0.19 | 1.05 | 0.28 |
| AC3-HTT | | 108 | 0.545 | 10.1 | 0.630 | 100 | 70 | 11 | 0.08 | 1.15 | 0.12 |
| AC3-HTT-T | | 83 | 0.698 | 16.9 | 0.780 | 73 | 68 | 51 | 0.05 | 0.89 | 0.30 |
| GL | 16.5 | 174 | 0.433 | 5.0 | 0.490 | 205 | 191 | 40 | 0.09 | 1.36 | 1.03 |
| GL-T | | 288 | 0.704 | 4.9 | 0.735 | 283 | 242 | 126 | 0.16 | 0.97 | 0.38 |
| GL-HTT | | 224 | 0.470 | 4.1 | 0.525 | 193 | 148 | 147 | 0.12 | 0.77 | 0.28 |
| GL-HTT-T | | 200 | 0.667 | 6.6 | 0.700 | 188 | | 100 | 0.11 | 0.92 | 0.45 |

carbon deposits $C_C$ were determined gravimetrically from the differences between weights of dry samples before and after thermal treatment at 500 °C in air.

**(b) Transmission Electron Microscopy.** TEM micrographs of carbosil samples were made with a BS 540 (Tesla) apparatus (accelerating voltage 80 kV, resolution 0.8 nm, magnification ×24 000). Microscope samples were prepared by the platinum−carbon replication method with evaporation of carbon and platinum onto the adsorbent surface then treated in hydrofluoric acid to dissolve oxides.

**(c) Nitrogen Adsorption−Desorption.** The specific surface area $S_{BET}$,[10] pore volume $V_p$ (estimated at $p/p_0 \approx 0.98$, where $p$ and $p_0$ denote the equilibrium and saturation pressures of nitrogen, respectively), average pore radii $R_p$, and other pore parameters listed in Table 1 were determined from nitrogen adsorption−desorption at 77.35 K measured with a Sorptomat 1900 (Carlo Erba, Milan) apparatus or a Micromeritics ASAP 2010 adsorption analyzer. Additionally, the total pore volume $V_\Sigma$ was evaluated using titration method[3] with methanol as a titrant added to weighted dry sample. The endpoint of titration was reached when powdered adsorbent lost its free-flowing character due to wetness. Typically, $V_\Sigma$ is slightly larger than $V_p$ (Table 1).

The micropore parameters ($V_{DS}$, $S_{DS}$) were estimated using the modified Dubinin−Stoeckli equation[11]

$$a = \frac{W_0}{2ZV^*}\exp\left(\frac{-mx^2_{DS}A^2}{Z^2}\right)^n\left[1 + \mathrm{erf}\left(\frac{x_{DS}}{\delta Z\sqrt{2}}\right)\right] \qquad (1)$$

where $x_{DS}$ is the pore half-width; $\delta$ is the distribution dispersion ($\delta_{DS}$ in Table 1); $Z = (1 + 2m\delta^2A^2)^{0.5}$; $m = (\beta k)^{-2}$; $\mathrm{erf}(z) = (2/\sqrt{\pi})\int_0^z e^{-t^2}\,dt$; $n$ is the varied equation parameter; $A = RT\ln(p_0/p)$ is the differential molar work equal, with inverse sign, to the variation in the Gibbs free energy; $\beta_{N2} = 0.33$; and $k = 10$ kJ nm/mol. The micropore parameters were computed without correction on the adsorption in mesopores, as integration for $S_{DS}$ and $V_{DS}$ was performed at $R_p < 1$ nm (however, this approach can result in some overestimation of the $S_{DS}$ and $V_{DS}$ values). The specific surface area of mesopores ($S_{mes}$) was computed with the theory of capillary condensation−evaporation with Broekhoff−deBoer−Dollimore−Heal−Dubinin−Ulin corrections to the Kelvin equation,[12,13] which links the adsorbed layer thickness ($t$) and the radius ($R_p > 1$ nm) of filled pores (empted on desorption), using the direct minimization method with the program package described in detail elsewhere.[14]

The Fowler−Guggenheim (FG) equation describing localized monolayer adsorption with lateral interaction[10,15]

$$\theta_l(p,E) = \frac{Kp\,\exp(zw\Theta/k_BT)}{1 + Kp\,\exp(zw\Theta/k_BT)} \qquad (2)$$

(where $K = K_0(T)\exp(E/k_BT)$ is the Langmuir constant, $z$ is the number of nearest neighbors of an adsorbate molecule (assuming $z = 4$), $w$ is the interaction energy between a pair of nearest neighbors, $k_B$ is the Boltzmann constant, and $zw/k_B = 380$ K[15] close to the liquefaction heat $Q_L$) was used as a kernel $\Theta_l$ in the overall adsorption isotherm in the form of a Fredholm integral

(10) (a) Adamson, A. W.; Gast, A. P. *Physical Chemistry of Surface*, 6th ed.; Wiley: New York, 1997. (b) *Characterization of Porous Solids*; Gregg, S. J., Sing, K. S. W., Stoeckli, H. F., Eds.; Soc. Chem. Industry: London, 1979. (c) Gregg, S. J.; Sing, K. S. W. *Adsorption, Surface Area and Porosity*, 2nd ed.; Academic Press: London, 1982. (d) Fenelonov, V. B. *Porous Carbon;* Nauka: Novosibirsk, 1995.

(11) Dubinin, M. M.; Stoeckli, F. *J. Colloid Interface Sci.* **1980,** *75*, 34.

(12) (a) Dollimore, D.; Heal, C. R. *J. Appl. Chem.* **1964,** *14*, 109. (b) Broekhoff, J. C.; deBoer, J. H. *J. Catal.* **1967,** *9*, 8; **1968,** *10*, 153.

(13) Dubinin, M. M.; Kataeva, L. I.; Ulin, B. I. *Izv. AN USSR, Ser. Khim.* **1977,** *No. 3*, 510.

(14) (a) Gun'ko, V. M. *Zh. Fiz. Khim.* **1989,** *63*, 506. (b) Gun'ko, V. M.; Lukyanchuk, V. M.; Chuiko, A. A. *Catal. Catal.* **1992,** *No. 28*, 82. (c) Gun'ko, V. M. *Teoret. Eksperim. Khim.* **2000,** *36*, 1.

(15) (a) Hill, T. L. *Statistical Thermodynamics;* McGraw-Hill: New York, 1956. (b) Choma, J.; Jaroniec, M. *Langmuir* **1997,** *13*, 1026. (c) Jaroniec, C. P.; Jaroniec, M.; Kruk, M. *J. Chromatogr. A* **1998,** *797*, 93.

equation of the first kind

$$\Theta(T, p) = \int_o^{y_{max}} \Theta_l(T, p, y)\, f(y)\, dy \quad (3)$$

where *f(y)* is the unknown distribution function of a given parameter $y$ (e.g., $y = E$ or $R_p$). A maximal $p/p_0$ value for an isotherm portion used with eq 2 corresponds to nearly monolayer coverage. To calculate the *f(y)* functions with the overall isotherm equation, a constrained regularization method can be used, as the solution of eq 3 is a well-known ill-posed problem due to the impact of noise on measured data, which does not allow one to utilize exact inversion formulas or iterative algorithms.[16,17] For this purpose, the constrained regularization CONTIN procedure[17] was modified to apply different local isotherm equations to estimate the distributions of the pore size and adsorption energy.

The pore size distribution was calculated by using the overall isotherm equation[18]

$$a = \int_{r_{min}}^{r_k(p)} f(R_p)\, dR_p + \int_{r_k(p)}^{r_{max}} \frac{w}{R_p} t(p, R_p) f(R_p)\, dR_p \quad (4)$$

where $r_{min}$ and $r_{max}$ are the minimal and maximal half-width or the pore radius, respectively; $w = 1$ for slitlike pores and 2 for cylindrical pores;

$$r_k(p) = \frac{\sigma_s}{2} + t(p,R_p) + \frac{w\gamma v_m \cos\theta}{R_g T \ln(p_0/p)} \quad (5)$$

$$t(p,R_p) = \frac{a_m\,[1 + (nb/2 - n/2)z^{n-1} - (nb + 1)z^n + (nb/2 + n/2)z^{n+1}]}{S_{BET}\quad [1 + (c - 1)z + (cb/2 - c/2)z^n - (cb/2 + c/2)z^{n+1}]} \quad (6)$$

$b = \exp(\Delta\epsilon/R_gT)$; $\Delta\epsilon$ is the excess of the evaporation heat due to the interference of the layering on the opposite wall of pores; $t(p,R_p)$ is the statistical thickness of adsorbed layer; $a_m$ is the BET monolayer capacity; $c = c_s \exp((Q_p - Q_s)/R_gT)$; $c_s$ is the BET coefficient for adsorption on flat surface $c_s = \gamma e^{(E-Q_L/RgT)}$, $Q_L$ is the liquefaction heat, $E$ is the adsorption energy, and $\gamma$ is a constant; $Q_s$ and $Q_p$ are the adsorption heat on flat surface and in pores, respectively; $z = p/p_0$; $n$ is the number (noninteger) of statistical monolayers of adsorbate molecules and its maximal value for a given $R_p$ is equal to $(R_p - \sigma_S/2)/t_m$; $t_m = a_m/S_{BET}$; and $\sigma_s$ is the collision diameter of surface atoms. Desorption data (total isotherms) were utilized to compute the $f(R_p)$ distribution with eq 4 and the regularization procedure under nonnegativity condition with a fixed regularization parameter $\alpha = 0.01$. According to Nguyen and Do,[18] eqs 4 and 6 are valid not only for mesopores but also for micropores (in ref 18, $x_{min} = 0$, but micropores at the half-width $x_{min} < 0.2$ nm are inaccessible for nitrogen molecules, therefore one can assume $x_{min} = 0.2$ nm in eq 4 that has not an influence on the positions of $f(R_p)$ peaks). Several models of pores were applied for silica gel and carbosils, such as cylindrical pores for silica gel, slitlike pores at $R_p < 2t_m$ for pyrocarbon, and pores as the gaps between spherical pyrocarbon particles themselves and between these particles and silica gel globules. In the last case, eq 5 should be replaced by[10c]

$$\ln\frac{p_0}{p} = \frac{\gamma v_m}{R_g T}\left[\frac{1}{r} - \frac{2}{\sqrt{(R + t' + r)^2 - R^2} - r + R + t'}\right] \quad (7)$$

where $R$ is the radius of pyrocarbon particles and $t' = t + \sigma_s/2$. Notice that the pore models have only a slight influence on the distribution functions computed with eqs 3−7.

The $f(R_p)$ distributions determined with eq 4 and linked to $dV_p/dR_p$ can be easily transformed to the distributions $f_S(R_p)$ with respect to the derivative of the specific surface area $dS/dR_p$ using the corresponding models of pores; e.g., for cylindrical pores

$$f_s(R_p) = \frac{2}{R_p}\left(f(R_p) - \frac{V_p}{R_p}\right) \quad (8)$$

A similar regularization procedure for the overall isotherm equation was usefully applied to compute the structural parameters of pores of modified silica gels and carbons.[19] Notice that standard calculations of the pore size distributions ($dV_p/dR_p$ or $dS/dR_p$ versus $R_p$) using the Barrett−Joyner−Halenda (BJH),[20] deBoer,[10,21] and Derjaguin−Broekhoff−deBoer−Dollimore−Dubinin−Ulin[13] equations gave incomplete pictures of the pore size distributions.[7,8,19] At the same time, the regularization procedure CONTIN with eq 4 provides more detailed distribution functions $f(R_p)$, which allow one to explore changes in micropores ($R_p < 1$ nm), mesopores (1 nm $< R_p <$ 50 nm), and transport pores at $R_p > 50$ nm caused by different pretreatments of silica gels and carbosils. Additionally, the $f(R_p)$ distributions computed with eq 4 are close to those calculated with the DFT method,[19g] but the last gave the distributions (for silica gels and carbons) close to those computed with eq 4, using only a portion of the isotherms at $p/p_0 > 0.01$.

**(d) NMR Investigation.** The $^1$H NMR spectra were recorded using a high-resolution WP-100 SY (Bruker) NMR spectrometer with a bandwidth of 50 or 15 kHz. The isotropic value of the chemical shift of $^1$H ($\delta_{H,iso}$) was referenced to tetramethylsilane (TMS). For water adsorbed on the silica surfaces from the gas phase, the chemical shifts were measured in $CDCl_3$ media. Relative mean errors were ±10% for signal intensity and ±1 K for temperature. The technique of freezing-out of water was applied to separate bulk and interfacial waters in the aqueous suspensions of silica gels or to distinguish different water layers on the adsorption from the gas phase.[22−25] The amounts of the interfacial unfrozen water ($C_{ufw}$) in the aqueous suspensions of silica gels were estimated by comparison of an integral intensity ($I_{ufw}$) of the $^1$H NMR signal of unfrozen water with that ($I_c$) of water adsorbed on oxide from the gas phase using a calibrated function $I_c = f(C^c)$, assuming $C_{ufw} = (C^c I_{ufw}/f(C^c))$, or by comparison of the water signals for liquid and gas phases at 285 K. The signals of surface hydroxyls and water molecules from ice were not detected due to features of the measurement technique and the short time ($\sim 10^{-6}$ s) of cross-relaxation of protons in solids.

The free surface energy ($\gamma_S$ in mJ/m$^2$) was calculated (with relative mean error ±15%) using the known dependence of changes in the Gibbs free energy of ice on temperature

$$\Delta G_i = 0.036(273 - \Gamma) \quad (9)$$

One can assume that water is frozen ($T < 273$ K) at the interfaces when $G = G_i$ and the value of $\Delta G = G_0 - G$ equals to $\Delta G_i = G_i|_{T=273K} - G_i(T)$ and corresponds to a decrease in the Gibbs free energy of the interfacial water due to its interaction with the solid surfaces ($G_0$ denotes the Gibbs free energy of the bulk undisturbed water and $\Delta G > 0$; i.e., the Gibbs free energy of the

(16) Szombathely, M.v.; Brauer, P.; Jaroniec, M. *J. Comput. Chem.* **1992,** *13*, 17.
(17) Provencher, S. W. *Comput. Phys. Commun.* **1982,** *27*, 213; 229.
(18) (a) Nguyen, C.; Do, D. D. *Langmuir* **1999,** *15*, 3608. (b) Nguyen, C.; Do, D. D. *Langmuir* **2000,** *16*, 7218.

(19) (a) Gun'ko, V. M.; Leboda, R.; Zarko, V. I.; Marciniak, M.; Chibowski, E. *Colloid. Surf. A*, submitted for publication. (b) Gun'ko, V. M.; Leboda, R.; Skubiszewska-Zięba, J.; Rynkowski, J. *J. Colloid Interface Sci.* **2000**, *231*, 13. (c) Gun'ko, V. M.; Leboda, R.; Grzegorczyk, W.; Scubiszewska-Zieba, J.; Marciniak, M.; Malygin, A. A.; Malkov, A. A. *Langmuir* **2000,** *16*, 3227. (d) Gun'ko, V. M.; Leboda, R.; Charmas, B.; Villieras, F. *Colloid Surf. A* **2000,** *173*, 159. (e) Leboda, R.; Gun'ko, V. M.; Marciniak, M.; Malygin, A. A.; Malkin, A. A.; Grzegorczyk, W.; Trznadel, B. J.; Pakhlov, E. M.; Voronin, E. F. *J. Colloid Interface Sci.* **1999,** *218*, 23. (f) Gun'ko, V. M.; Villiéras, F.; Leboda, R.; Marciniak, M.; Charmas, B.; Skubiszewska-Zięba, J. *J. Colloid Interface Sci.* **2000,** 230, 320. (g) Gun'ko, V. M.; Do, D. D. *Colloids Surf. A*, in press.
(20) Barrett, E. P.; Joyner, L. G.; Halenda, P. P. *J. Am. Chem. Soc.* **1951,** *73*, 373.
(21) Toth, J. *Adv. Colloid Interface Sci.* **1995,** *55*, 1.
(22) Gun'ko, V. M.; Turov, V. V. *Langmuir* **1999,** *15*, 6405.
(23) Gun'ko, V. M.; Zarko, V. I.; Turov, V. V.; Leboda, R.; Chibowski, E. *Langmuir* **1999,** *15*, 5694.
(24) Turov, V. V.; Leboda, R. *Adv. Colloid Interface Sci.* **1999,** *79*, 173.
(25) Leboda, R.; Turov, V. V.; Marcyniak, M.; Malygin, A. A.; Malkov, A. A. *Langmuir* **1999,** *15*, 8441.

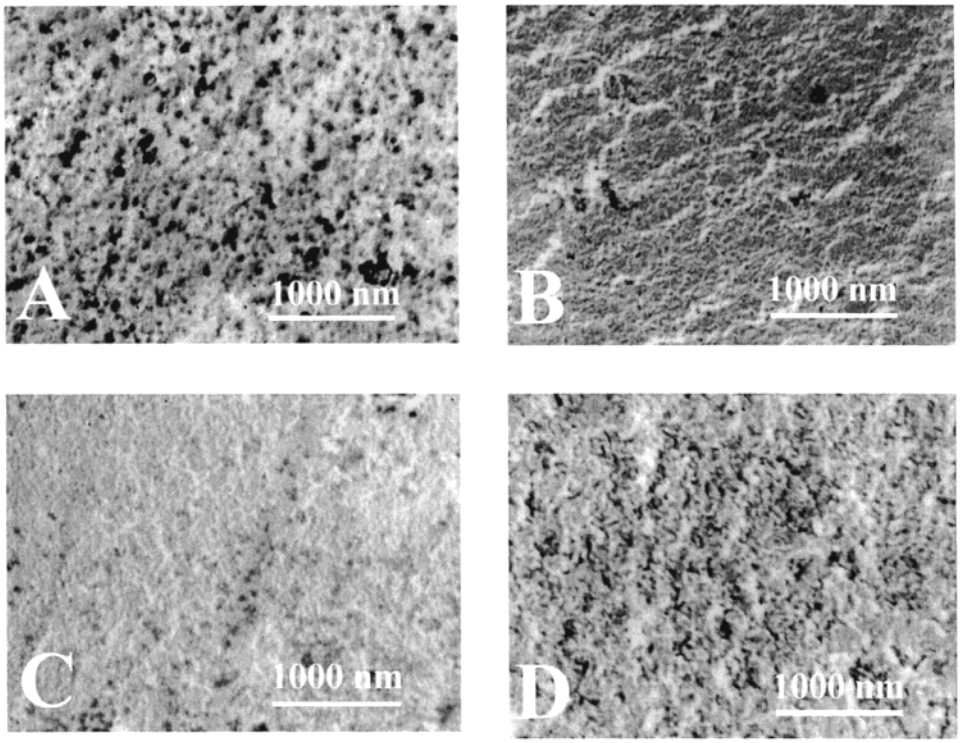


**Figure 1.** TEM micrographs of (a) Si-60, (b) Si-60-T, (c) Si-60-HTT at $T_{HTT}$ = 150 °C, and (d) Si-60-HTT at $T_{HTT}$ = 200 °C.

interfacial water is lower than that of the bulk water). On the basis of this approach, one can estimate the concentrations of strongly ($C^s_{ufw}$) and weakly ($C^w_{ufw}$) bound unfrozen waters, a maximal reduction of the Gibbs free energy of strongly and weakly bound waters ($\Delta G^s$ and $\Delta G^w$), and free surface energy of adsorbent in aqueous medium ($\gamma_S$)

$$\gamma_S = K\int_0^{C^{max}_{ufw}} \Delta G \, dC_{ufw} \tag{10}$$

where $K$ is a constant and $C^{max}_{ufw}$ is the total amount of unfrozen water at T → 273 K. The $\Delta G$ value in eq 10 is the differential Gibbs free energy, which is equal to the differential work of adhesion

$$\Delta G = -W_a \tag{11}$$

Therefore $\gamma_S$ equals the total work of adhesion related to the interface between the oxide and liquid phases. The force of adhesion (per meter squared of the oxide surface) can be calculated by a simple equation

$$F = \Delta G / X \tag{12}$$

where $X$ is the distance from the surface. For cylindrical pores in silica gels, $X$ can be estimated as follows

$$X = R_p\left[1 - \left(1 - \frac{C_{ufw}}{\rho_{ufw} V_p}\right)^{0.5}\right] \tag{13}$$

assuming that the specific density of water in pores ($\rho_{ufw}$) is equal to ≈1 g/cm$^3$ and for a flat surface (or large pores)

$$X = 3C_{ufw}/S \tag{14}$$

## Results and Discussion

The Si-60 surface seems rough and granular and globules forming large particles (0.1−0.2 mm) of silica gel are observed (Figure 1a) as well as large transport pores (dark areas in micrographs); however, main mesopores of Si-60 at $R_p$ < 10 nm are invisible due to relatively low TEM magnification (24 000). After heating at 500 °C for 24 h in air, the silica gel surface appears slightly smoother, and granular structure is less visible (Figure 1b); however, significant changes in the pore characteristics do not occur (Table 1). After hydrothermal treatment (HTT) of Si-60 at 150 °C for 6 h, the silica surface becomes spongy (Figure 1c) and the specific surface area of both mesopores and micropores significantly decreases; however, $V_p$ is nearly the same. After HTT at 200 °C, the spongy character of the surface becomes more clearly visible (Figure 1d), and $V_p$ and $S_{BET}$ (as well as $S_{mes}$, $S_{DS}$, etc.) decrease strongly due to enlargement of pores and reduction of their number because of disruption of the pore walls on the intensive hydrolysis of Si−O−Si bonds.[26]

Pyrocarbon grafting on the silica gel surfaces results in formation of both relatively large and practically nonporous carbon particles (Figure 2a,b) and a carbon layer with smaller graphene particles on the silica surfaces (Figure 2c). Both processes lead to reduction of the porosity and the specific surface area (as well as the accessibility of pores blocked by carbon deposits) due to pore filling by pyrocarbon (Table 1), as the last formed from precursors of small molecular sizes (under the used pyrolysis conditions) possesses low porosity (close to that of carbon black).[19,27] Additionally, the oxide matrix can be changed during the pyrolysis due to chemical reactions with precursor molecules or pyrolysis products (especially water molecules formed from oxygen-containing reactants). For example, the glucose carbonization is accompanied by the largest changes in the pore structure among prepared carbosils (Table 1, GL). Notice that pyrocarbon includes not only pure graphene structures but also oxidized groups, such as C═O, COH, C−O−C, and COOH, which can impact the adsorptive properties of carbosils as the whole or their particle characteristics in the aqueous suspensions.[19,27]

(26) Kiselev, A. V.; Lygin, V. I. *IR Spectra of Surface Compounds and Adsorbed Substances*, Nauka: Moscow, 1972.

(27) Gun'ko, V. M.; Skubiszewska-Zieba, J.; Leboda, R.; Zarko, V. I. *Langmuir* **2000,** *16,* 374.

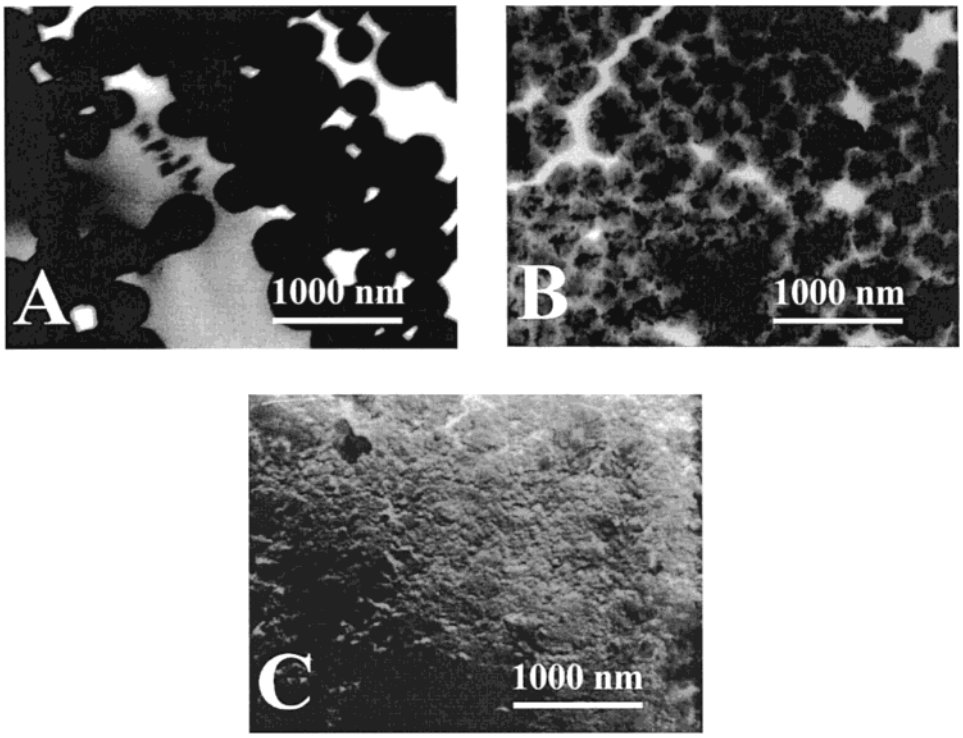


**Figure 2.** TEM micrographs for (a) AC3, (b) GL, and (c) AN2.

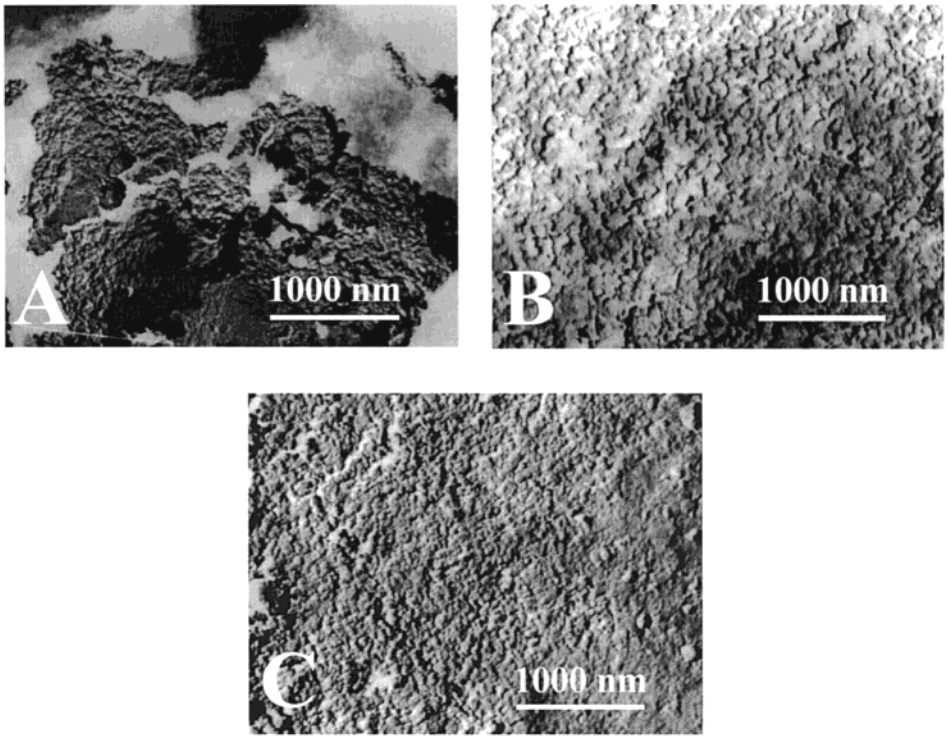


**Figure 3.** TEM micrographs for (a) GL-HTT, (b) AC3−HTT, and AN2−HTT

Hydrothermal treatment (HTT) of carbosils alters the pore parameters depending on $C_C$ (Table 1), due to shielding of the oxide surfaces by pyrocarbon deposits inhibiting hydrolysis of the silica pore walls (Figure 3a). However, marked differences in the surface structure in comparison with that of Si-60-HTT are not observed, e.g., for AC3-HTT and AN2-HTT (Figure 1c and 3b,c). Similar results are found for samples after HTT and subsequent heating at 500 °C in air (HTT-T) (Figure 4) depending on the HTT temperature ($T_{HTT}$), which was higher for AC*i* samples. Thus, shielding of the oxide matrix by pyrocarbon is responsible for smaller reduction of the specific surface area on HTT and HTT-T in comparison with that for Si-60-HTT and Si-60-HTT-T (Table 1).

The carbosil surfaces after heating at 500 °C for 24 h (Figure 4) are akin to those of Si-60-T (Figure 1b); however, *S* and *V* (Table 1) are smaller for carbosils than for Si-60-T due to chemical transformations of the pore walls during pyrolysis, especially for glucose containing large number of hydroxyls (which lead to the hydrolysis of Si−O−Si bonds in the pore walls). On the other words, glucose carbonization is accompanied, in fact, by HTT of

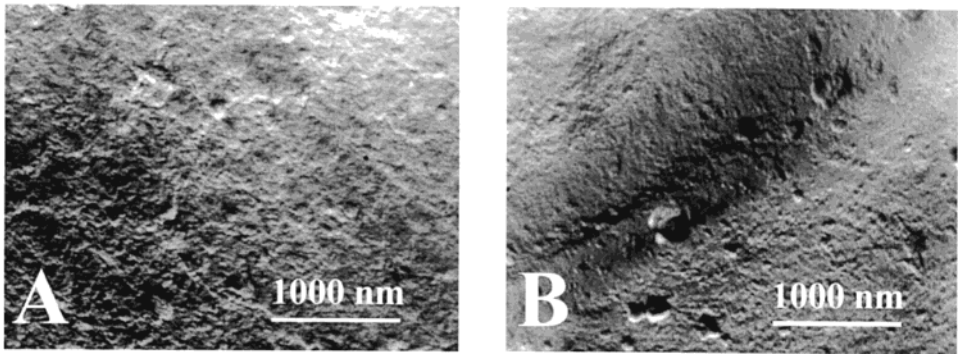


**Figure 4.** TEM micrographs for (a) AN2-T and (b) GL-T.

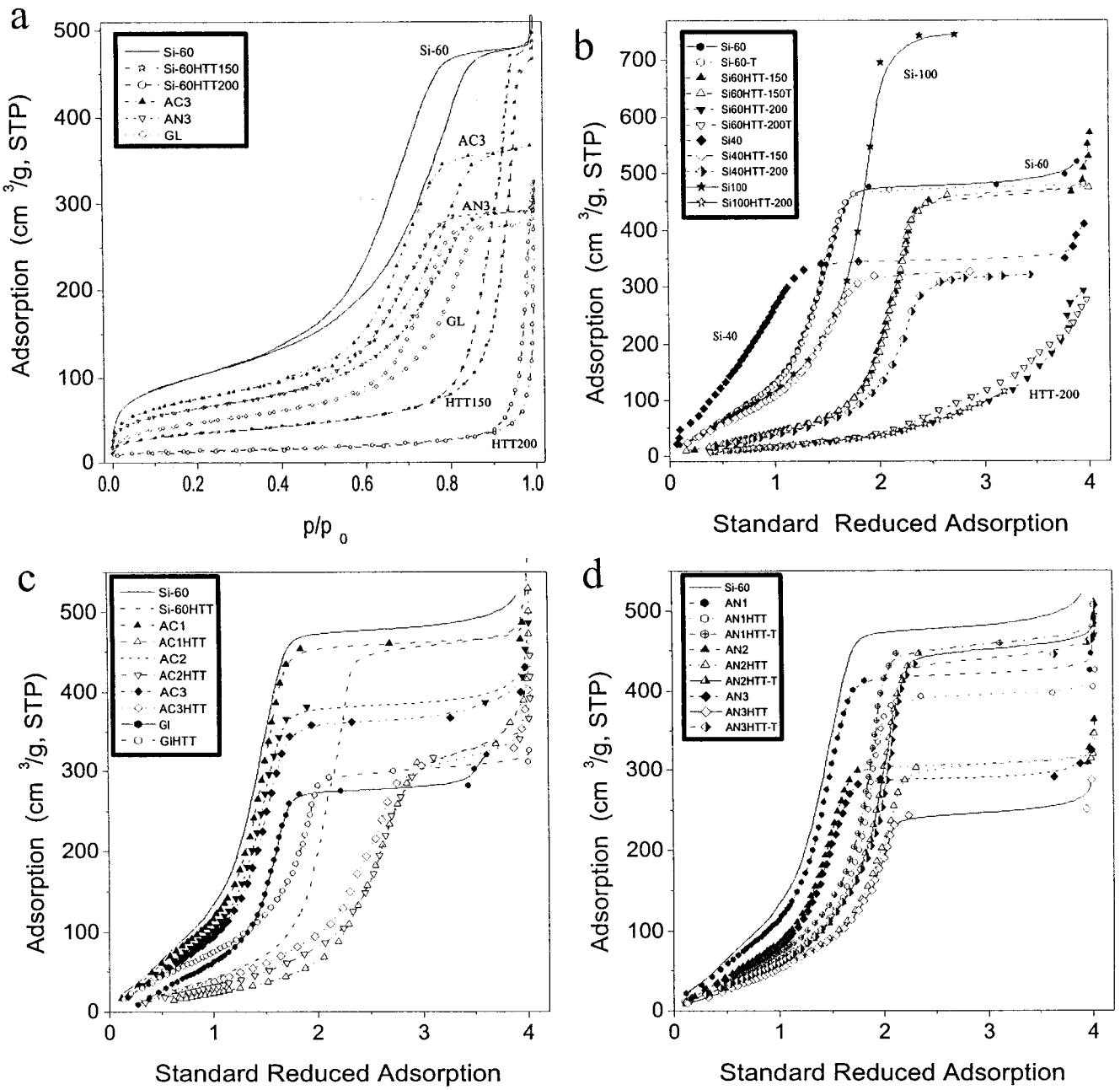


**Figure 5.** (a) Nitrogen isotherms for Si-60, initial and modified, and the $\alpha_S$ plots for (b) Si-60, Si-40, and Si-100 pristine and treated, (c) initial and treated Aci and GL, and (d) initial and treated ANi.

silica gel and the GL-T surface seems close to that of Si-60-HTT.

The $\alpha_S$ plots[10] for silica gels and carbosils (Figure 5, reference adsorption corresponds to Si-1000[28]) show significant changes in the porosity due to different treatments of adsorbents. However, dramatic changes in the pore type are observed only after HTT at 200 °C of silica gels (Figure 5b) or ACi-HTT (Figure 5c). In the last

case, these changes are smaller due to shielding of the surfaces by pyrocarbon. For other samples, substantial alterations in the pore volume or the specific surface area (Table 1) can be rather due to blocking of pores by pyrocarbon particles, as the porosity of the last is low and the specific surface area of pyrocarbon per se is provided by the external surfaces of carbon particles. A visible displacement of the plateau adsorption toward larger $\alpha_S$ values for some modified samples (Figure 5) is linked to enlargement of the size of mesopores (Table 1, $R_p$), which are filled by nitrogen at higher $p/p_0$ (Figure 5a). All samples based on Si-60 demonstrate a low microporosity, as an initial linear part of their $\alpha_S$ plots does not have a steep increase and points toward the origin of the coordinates (Figure 5). Additionally, the specific surface area ($S_\alpha$) magnitudes determined on the basis of this portion of the $\alpha_S$ plots are close to both $S_{BET}$ and $S_{mes}$ (Table 1), and the micropore volume estimated with the $\alpha_S$ plots for all samples is less than 0.01 $cm^3/g$. The $V_{DS}$ and $S_{DS}$ values (Table 1) could be overestimated, as they were computed without correction of the isotherms on adsorption in mesopores. A steep increase in adsorption at $\alpha_S > 1$ for many of the samples (Figure 5) is linked with secondary filling of mesopores (capillary condensation corresponding to hysteresis loops, Figure 5a).

The pore volume and the specific surface area of carbosils decrease with $C_C$ independently of the origin of the pyrocarbon (Figure 6, Table 1). However, the precursor type and variations in pyrolysis conditions (temperature and time),[19] as well as the initial pore structure of silica gels (e.g., Si-40 and Si-60), impact the pore characteristics of carbosils (Figures 6 and 7). For example, the narrower the pores of the pristine silica gel, the larger the specific surface area reduction under the same pyrolysis conditions (Figure 5b, Si-40, average $R_p \approx 1.5$ nm and Si-60, $R_p \approx 4$ nm). Additionally, the pyrolysis of organics having oxygen atoms in molecules leads to a greater decrease in the specific surface area due to hydrolysis of Si−O−Si bonds and disruption of the pore walls (Figure 5, AC and GL). Notice that heating of Si-60 causes diminution of the half-width and dispersion of narrow pores (Table 1, $x_{DS}$, $\delta_{DS}$); i.e., micropores become more uniform. HTT of Si-60 (especially at 200 °C) not only enhances the mesopore sizes but also strongly disrupts micropores, as $S_{DS}$ and $V_{DS}$ decrease by several times (Table 1) and minimal $V_{DS}$ is observed for Si-60-HTT-T at $T_{HTT} = 200$ °C among all the studied samples; however, minimal $S_{DS}$ is for AC*i*-HTT at the same $T_{HTT}$. Changes in the pore structure as a whole due to different pretreatments of various carbosils (Table 1, Figures 5−7) can be elucidated in details analyzing the pore size distributions computed using the overall isotherm approximation with the regularization procedure.

The regularization procedure with eq 4 fits adsorption−desorption isotherms for all the samples in faithful agreement with experimental ones over the total $p/p_0$ range, which lends support to the validity of eq 4 for both micropores and mesopores. Additionally, the pore size distributions $f(R_p)$ of Si-60, Si-40, and Si-100 calculated with eq 4 and the regularization procedure (fixed regularization parameter $\alpha = 0.01$ and nonnegativity condition for $f(R_p)$) using desorption data are close to $dV_p/dR_p$ obtained with the frequently used Barrett−Joyner−Halenda (BJH) method at $R_p > 1$ nm (Figure 7b). However, eq 4 allows one also to compute $f(R_p)$ for micropores at $R_p$ < 1 nm, therefore subsequent calculations of $f(R_p)$ and $f_S(R_p)$ were performed only with eq 4. Notice that $f(R_p)$ computed with eq 4 using desorption data is between $dV_p/dR_p$(BJH) for adsorption and desorption, which is clearly seen for Si-100 (Figure 8). For all the studied samples based on Si-60, the $f(R_p)$ peaks for micropores are very narrow (notice that the log scale is used in Figures 8 and 9) and give a small contribution to the pore volume.

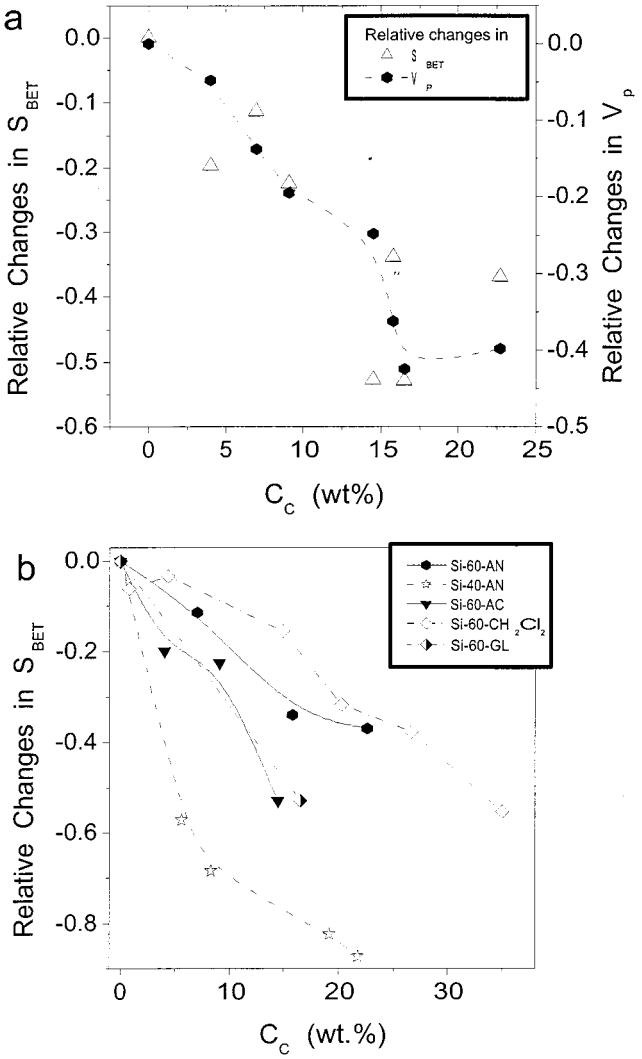


**Figure 6.** Relative changes in (a) $S_{BET}$ and $V_p$ for carbosils with Si-60 and (b) $S_{BET}$ for carbosils with Si-60 and Si-40 covered by pyrocarbon of different origin.

Heating of Si-60 at 500 °C (Si-60-T) results in slight narrowing of the main $f(R_p)$ peak at $R_p$ between 2 and 7 nm (Figure 9a). However, a small $f(R_p)$ peak at $R_p > 10$ nm shifts toward larger $R_p$ due to changes in the sizes of nanoscaled silica globules on heating and corresponding rearrangement of mesopores. HTT of Si-60 at 150 °C results in reduction of all $f(R_p)$ peaks ($V_p$ slightly decreases) and displacement of the main mesopore peak toward $R_p > 10$ nm (Figure 9a). HTT of Si-60 at 200 °C gives significant broadening of the pore size distribution, and subsequent heating of the last sample enhances this broadening (Figure 9b).

The origin and amounts of pyrocarbon impact the main mesopore $f(R_p)$ peak at $R_p > 2$ nm (Figure 9c). The greatest changes in mesopores and micropores (Table 1, Figure 9c) are observed for GL samples due to factual HTT of silica gel on the carbonization of glucose, which is a source of water molecules hydrolyzing Si−O−Si bonds in the pore

(28) (a) Jaroniec, M.; Kruk, M.; Olivier J. P. *Langmuir* **1999**, *15*, 5410. (b) Jaroniec, M.; Kruk, M.; Jaroniec, C. P.; Sayari, A. *Adsorption* **1999,** *5*, 39−45.

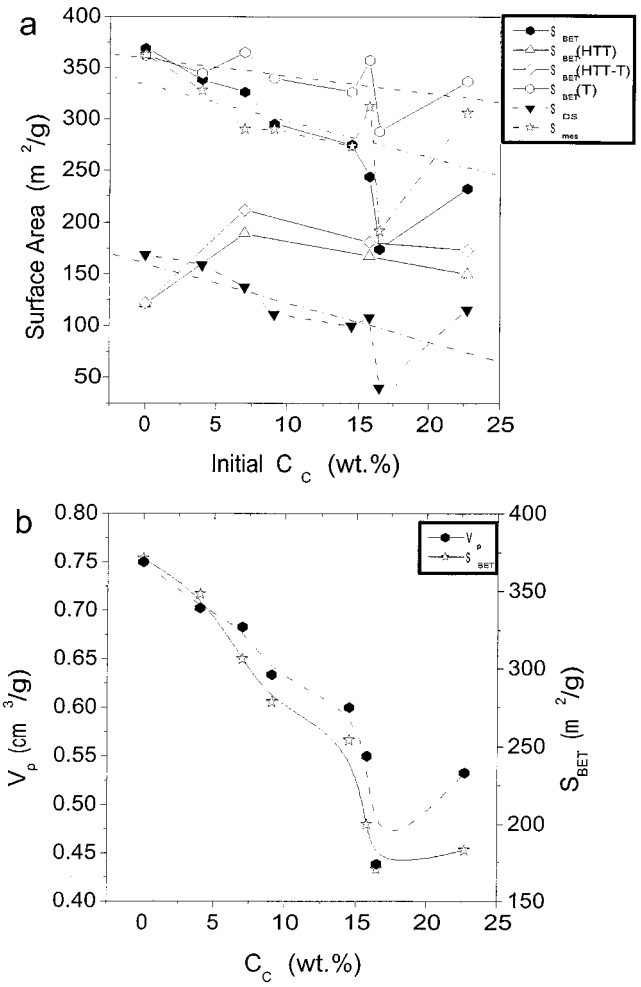


**Figure 7.** Specific surface area of (a) micropores ($S_{DS}$) and mesopores ($S_{mes}$) and $S_{BET}$ for treated samples as functions of the initial amounts of pyrocarbon and (b) pore volume of initial carbosils versus $C_C$.

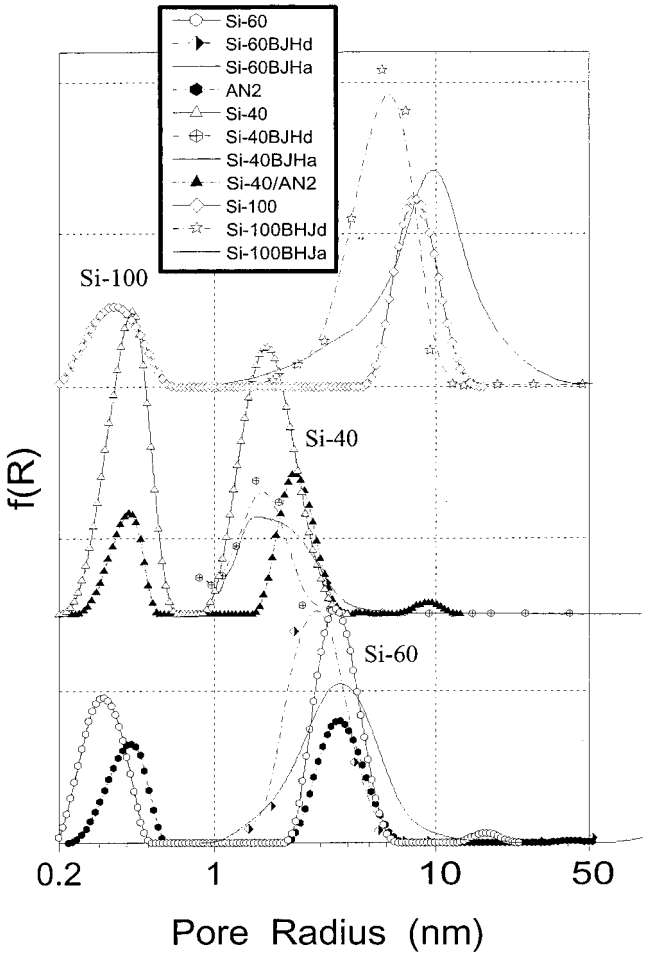


**Figure 8.** Pore size distributions for Si-60, Si-40, and Si-100 computed with eq 4 and BJH method using adsorption (BJHa) and desorption (BJHd) data; $f(R_p)$ for Si-60 and Si-40 modified by the pyrolysis of acenaphthene at close $C_C$ values are also shown.

walls. A similar effect is observed for AC*i* samples, but displacement of $f(R_p)$ for mesopores toward larger $R_p$ is smaller due to a lower number of oxygen atoms in acetylacetone in comparison with glucose. Minimal changes in mesopores are observed for AN*i* samples (aromatic $C_{12}H_{10}$ as a precursor); however, changes in $f(R_p)$ for micropores of AC*i* and AN*i* depend on $C_C$ larger than that for mesopores (Table 1) due to alteration in pyrocarbon distribution in matrix pores and on outer surfaces of silica gel particles in the form of relatively large globules (Figures 2−4).

Heating of carbosils at 500 °C for 24 h in air gives $f(R_p)$ different from that for Si-60-T (Figure 9f). Consequently, pyrolysis of various precursors under the same conditions is accompanied by distinct changes in the matrix pore structure, which are reflected by incomplete resuming of pores on oxidizing of carbon deposits in air at 500 °C, especially for GL-T (Figure 9f, Table 1).

Significant changes in the pore structure of adsorbents are observed due to their hydrothermal treatment (Figure 9d). An increase in $T_{HTT}$ for Si-60 from 150 °C (main portion of mesopores at $R_p$ between 7 and 25 nm) to 200 °C gives larger pores up to 200 nm with a very broadened distribution. In the case of AN*i* samples, pore enlargement due to HTT is less than that for AC*i* (Figure 9d) because of the differences not only in $T_{HTT}$ but also in the pyrocarbon deposit characteristics (one prepared with acetylacetone or glucose can include a large number of oxidized groups in contrast to pyrocarbon prepared by the carbonization of pure aromatics without O atoms in the molecules) and modified (hydrolyzed) oxide pore walls. These effects reflect in the mesopore and micropore parameters of AN*i*-HTT and AC*i*-HTT samples (Table 1) showing larger changes in AC*i* samples; i.e., pyrocarbon in AN*i* and GL samples shields the oxide surfaces on HTT at 150 °C strongly than that for AC*i* on HTT at 200 °C. It seems likely that HTT of AC*i* at higher temperature has larger effect than the difference in the origin of pyrocarbons. Subsequent heating of HTT-samples (HTT-T) results in smaller changes in the pore structure; however, mesopores become narrower (Figure 9e), as well as for pristine silica gel (Figure 9a, Table 1). For AN*i*-HTT-T samples, an increase in $S_{BET}$ and $V_p$ is observed, but for AC*i*-HTT-T, $S_{BET}$ decreases (Table 1).

The $f_S(R_p)$ distribution functions with respect to the specific surface area ($dS/dR_p$) show that main contribution to $S$ is given by pores at $R_p < 10$ nm (Figure 10). It should be noted that relative contribution of micropores to $S$ increases for all the samples after HTT, especially at $T_{HTT} = 200$ °C, with parallel disruption of main mesopores at $R_p$ between 2 and 6 nm. For carbosils, maximal contribution of micropores to $S$ is observed for AN1 and AC1 at low $C_C$ (Figure 10a).

Thus, the pore structure depends not only the pretreatment techniques but also on the origin of pyrocarbon (i.e., precursor composition). The last impacts the nitrogen

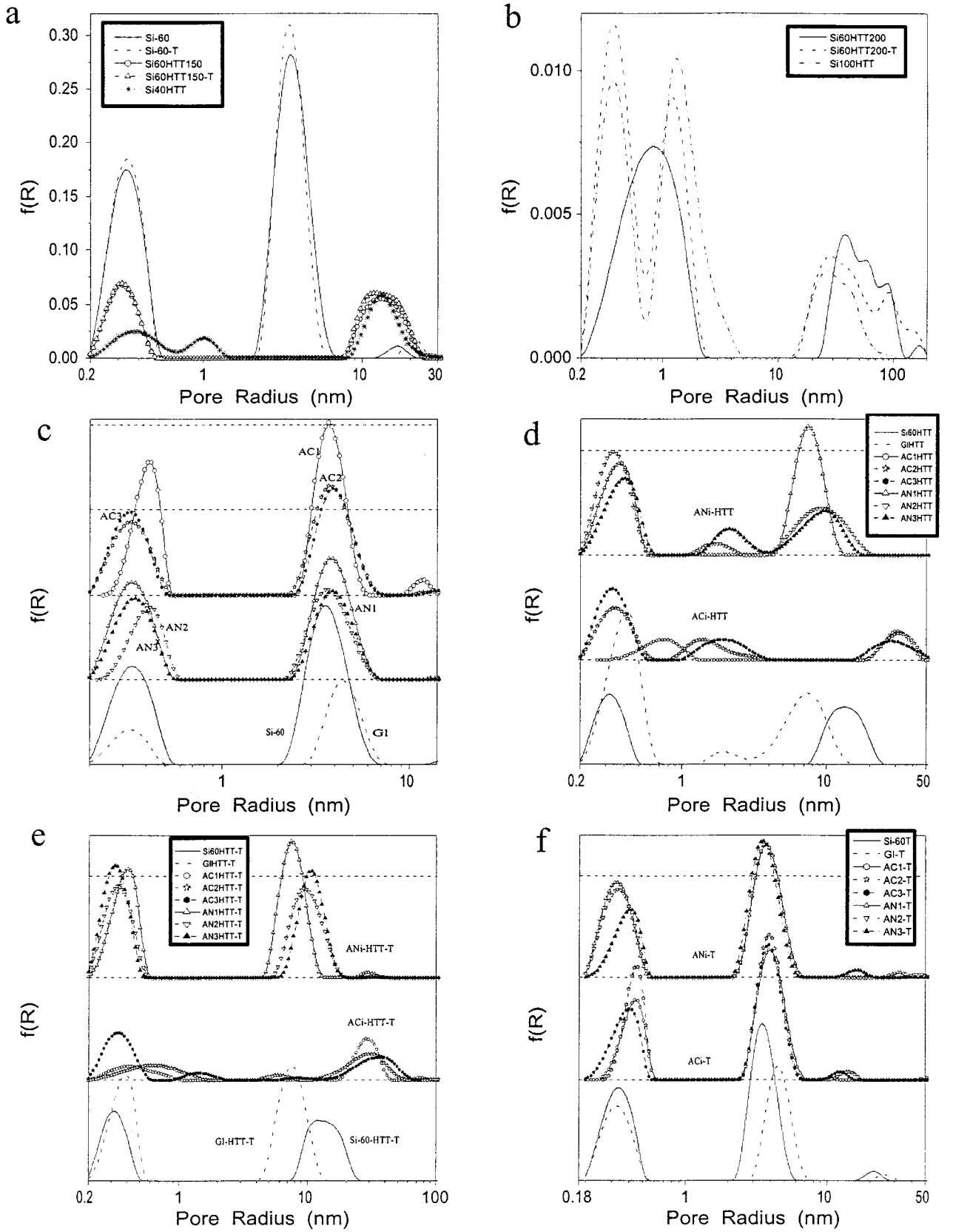


**Figure 9.** Pore size distribution computed with eq 4 with the regularization procedure ($\alpha = 0.01$) for (a) initial Si-60, Si-60-T, Si-60-HTT, and Si-40HTT at $T_{HTT}$ =150 °C; (b) Si-100-HTT, Si-60HTT at $T_{HTT}$ =200 °C and then heated at 500 °C for 24 h; carbosils (c) initial, (d) after HTT, (e) after HTT-T, and (f) after heating at 500 °C for 24 h.

adsorption energy distributions (Figure 11a) caused mainly by dispersion interaction (plus electrostatic contribution due to polarization of $N_2$ molecules interacting with polar oxide surfaces, e.g., silanols). For AN*i* and AC*i*, the $f(E)$ peak between 10 and 12 kJ/mol (adsorption in broad micropores or narrow mesopores) shifts toward higher energy with $C_C$ and it is markedly low for pristine silica gel due to changes in the micropore structure of adsorbent, as pores between primary silica gel globules and pores between graphene sheets possess different

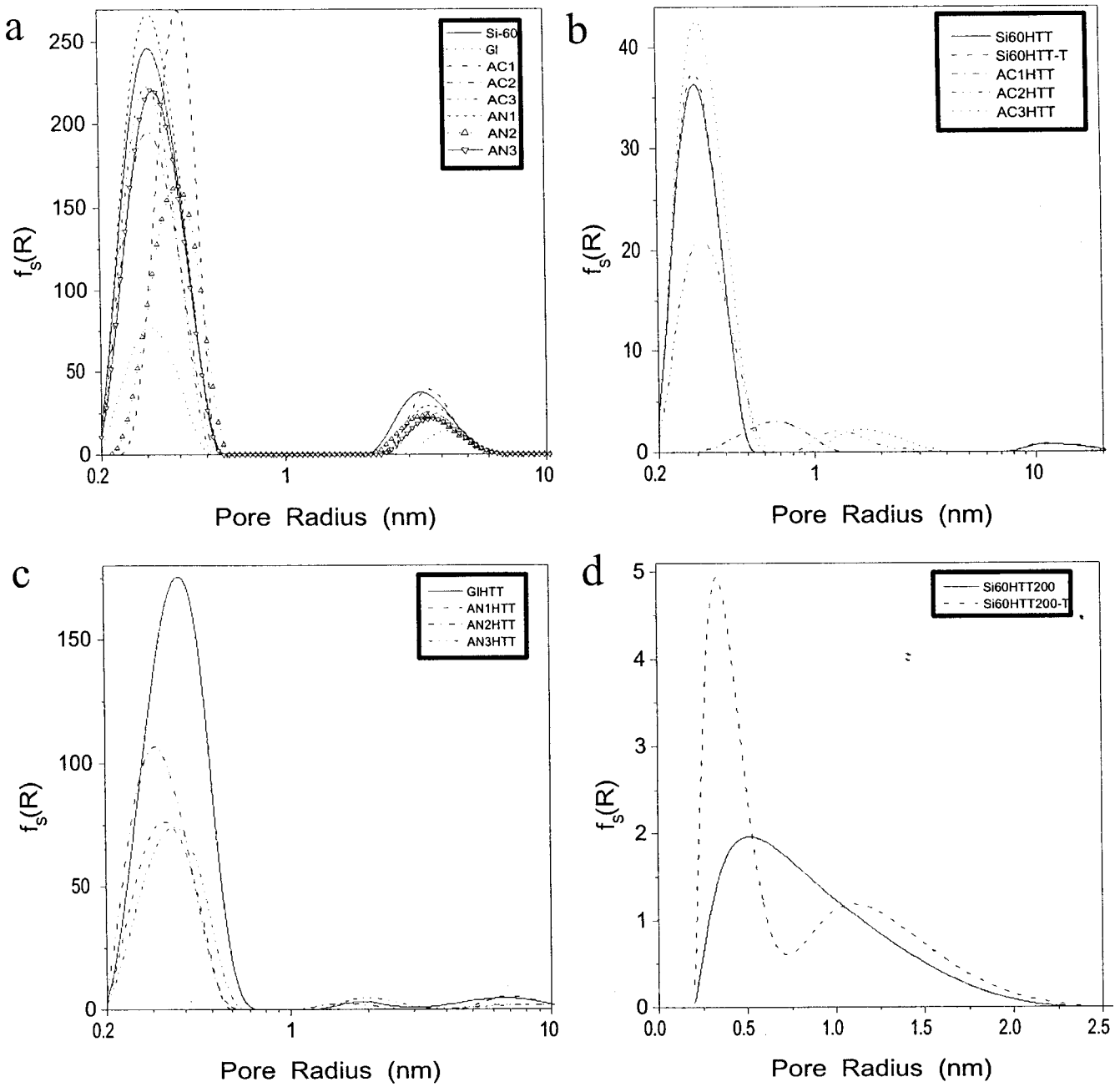


**Figure 10.** Pore size distribution with respect to $dS/dR_p$ for (a) initial Si-60 and carbosils, (b) Si-60 and ACi after HTT, (c) GL and ANi after HTT, and (d) Si-60 after HTT and HTT-T at $T_{HTT} = 200$ °C.

structural and absorptive characteristics.[10] Heating of Si-60 in air at 500 °C for 24 h results in small changes in $f(E)$, as the nature of the silica surfaces and pore structure are nearly the same; however, the $f(E)$ peak at 12 kJ/mol is larger due to a displacement of $f(R_p)$ for Si-60-T toward smaller $R_p$ for micropores. The $f(E)$ peak at ≈22 kJ/mol is linked with adsorption in the narrowest micropores at low $p/p_0$, and it is not shown for all samples as its intensity is very low. The $f(E)$ peak at ≈6 kJ/mol corresponds to adsorption in broad mesopores and can be linked with secondary (volume) filling of these pores at $p/p_0 > 0.1$[10,15,19] and, clearly, is practically independent of the nature of the surfaces. HTT and HTT-T give a small displacement of $f(E)$ peaks toward lower energy (Figure 12) due to enlargement of a major portion of pores and removal of carbon deposits.

Some structural features of different hydrothermally treated silica gels (Si-40, Si-60, Si-100) can be elucidated by using the $^1$H NMR method with freezing-out of adsorbed water at $T < 273$ K.[22−25] Vertical portions of the $\Delta G(C_{ufw})$ graphs (Figure 13a) are observed for the aqueous suspensions of initial silica gels Si-40 and Si-60 in contrast to nonporous adsorbents,[24] initial Si-100 (Figure 13a), and all hydrothermally treated samples (Figure 13b) possessing larger pores. Appearance of this portion of $\Delta G(C_{ufw})$ is due to unfreezing of the interfacial water in narrow pores with lowering temperature until $T$ corresponding to a maximal $\Delta G$ value for this plot portion. On the other words, lowering $T$ over some interval is not accompanied by water freezing, as this water is under strong action of the silica surfaces in narrow pores, when electrostatic fields of the opposite pore walls strongly overlap.[10] A similar effect was observed previously for water adsorbed on microporous carbons,[24,29] whose $\Delta G(C_{ufw})$ plots are akin to that for initial Si-40.

(29) Leboda, R.; Turov, V. V.; Tomaszewski, W.; Gun'ko, V. M.; Skubiszewska-Zięba, J. *Carbon*, in press.

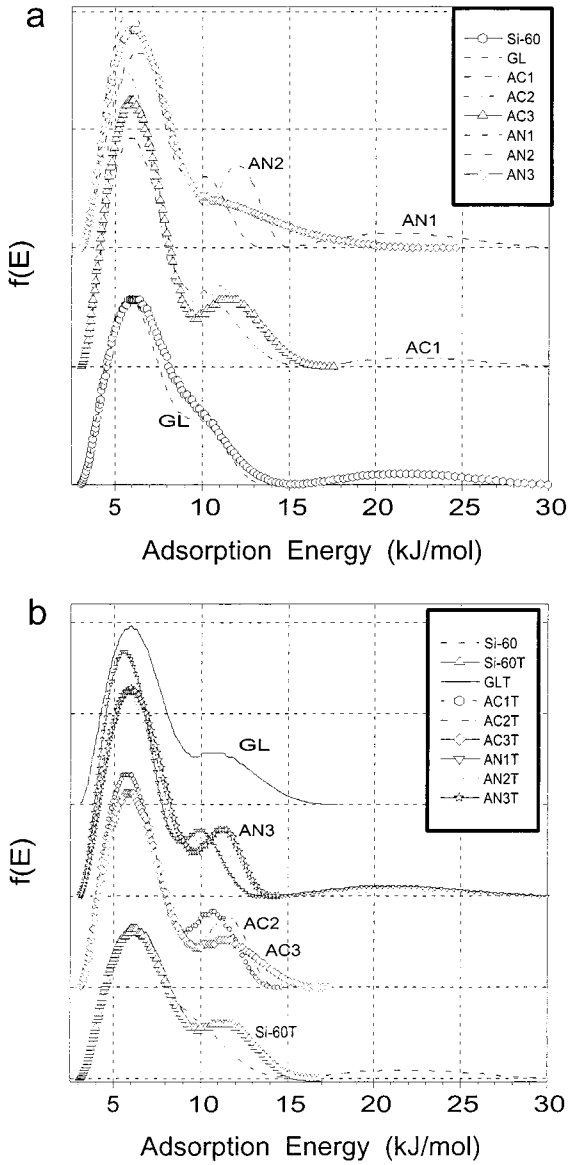


**Figure 11.** Nitrogen adsorption energy distribution calculated using eq 2 with the regularization procedure ($\alpha = 0.01$) for (a) initial silica and carbosils and (b) after heating at 500 °C for 24 h.

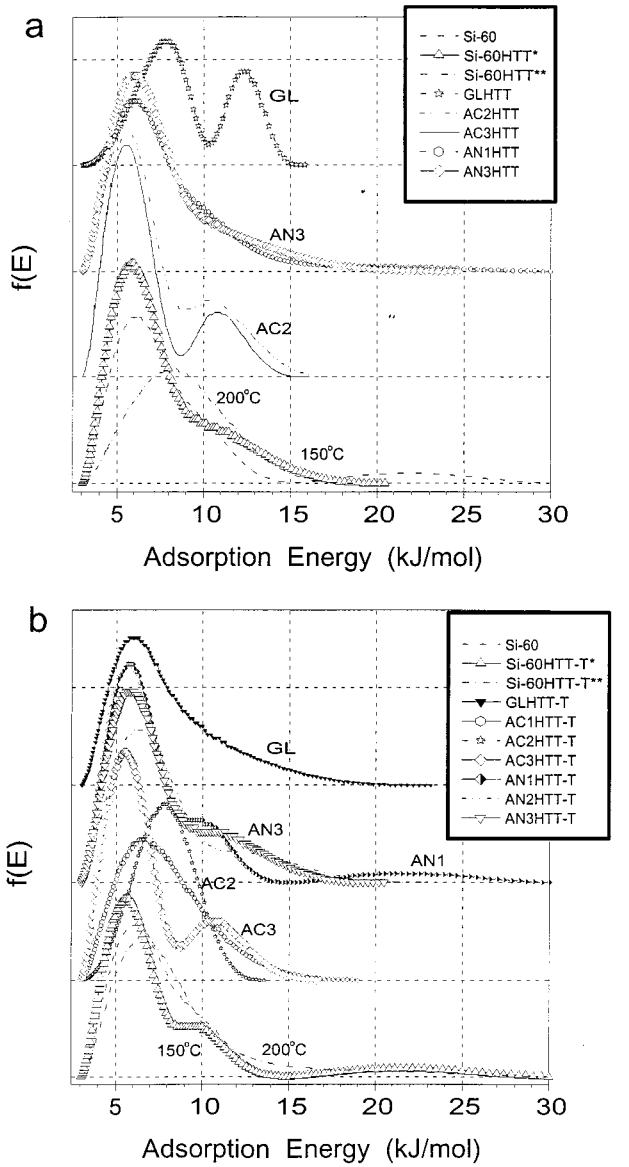


**Figure 12.** Nitrogen adsorption energy distribution computed using eq 2 with the regularization procedure ($\alpha = 0.01$) for silica gel and carbosils after (a) HTT and (b) HTT-T; *150 °C and **200 °C for Si-60.

The concentration of strongly bound water $C^s_{ufw}$ decreases with increasing pore size for both initial and hydrothermally treated silica gels (Table 2). The concentration of weakly bound water $C^w_{ufw}$ is larger for the HTT samples due to the enhancement of the pore size; however, the relationships between the $C^w_{ufw}$ values for different silica gels (initial and HTT) are more complex than those for $C^s_{ufw}$ (Table 2). Notice that the volume of unfrozen water for HTT-200 samples is larger than their pore volume, maybe due to formation of thick water layers on the outer surfaces of treated samples. Also, filling of large pores by nitrogen could be incomplete at $p/p_0 \approx 0.98$ (estimation of $V_p$ was made for this $p/p_0$), in contrast to filling by water in the aqueous suspensions.

The free surface energy $\gamma_S$ is maximal for Si-60, initial or HTT. There can be several reasons for this result, as the free surface energy at the silica/water interfaces depends on both the nature (e.g., concentration of silanols, charge density) and the topography of the surfaces. HTT for all samples leads to an increase in $\gamma_S$ but by different magnitudes, and $\Delta\gamma_S$ (changes in $\gamma_S$ due to HTT) is maximally (236 mJ/m$^2$) for Si-100HTT (Table 2). Additionally, HTT results in a marked enhancement of $\Delta G^s$, which characterizes the free energy of the first monolayer of adsorbed water. This value for HTT samples is significantly greater than that for other materials investigated previously,[24,30] which can be due to a substantial increase in the concentration of silanols ($\equiv Si-O-Si\equiv + H_2O \rightarrow \equiv SiOH + HOSi\equiv$) (concentration of silanols for different silicas in air can alter by several times[7]), capable of forming strong hydrogen bonds with water molecules from the first layer with a larger number of such bonds per a molecule; i.e., the number of strongly bound water molecules in the first layer increases for HTT samples. This circumstance leads to unusual behavior of the $\delta_H(T)$ functions for the HTT samples, as the average chemical shift decreases with increasing water concentration at a given temperature (Figure 14). However, for initial silica gels, the opposite result is observed. Notice that the $F(X)$ function correlates with increasing pore size for HTT

(30) Gun'ko, V. M.; Zarko, V. I.; Turov, V. V.; Leboda, R.; Chibowski, E.; Pachlov, E. M.; Goncharuk, E. V.; Marciniak, M.; Voronin, E. F.; Chuiko, A. A. *J. Colloid Interface Sci.* **1999,** *220*, 302.

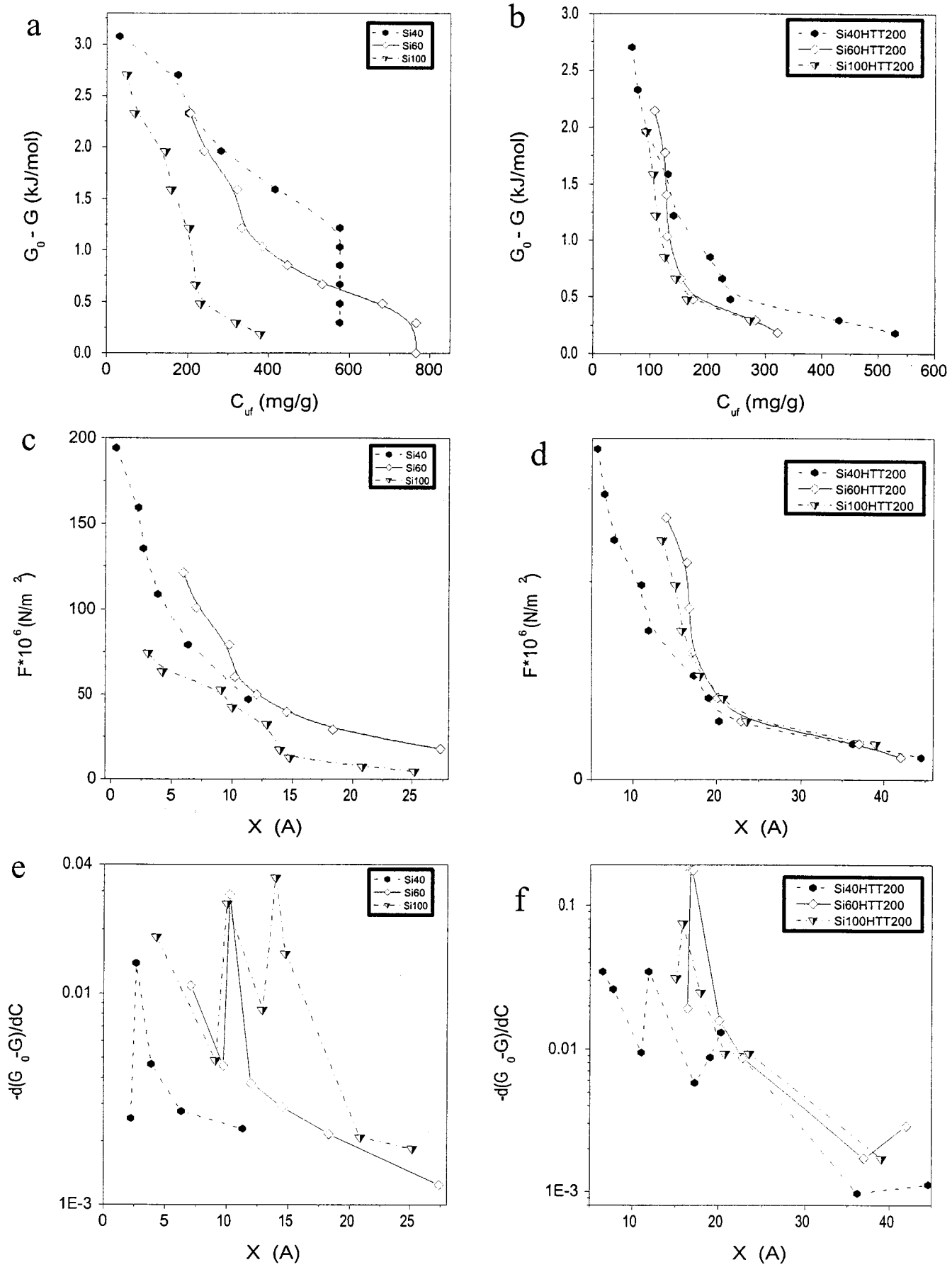


**Figure 13.** Changes in the Gibbs free energy of the interfacial water in the aqueous suspensions of initial (a) and hydrothermally treated (b) Si-40, Si-60, and Si-100 and corresponding adhesion forces (c, d) and derivatives $d(\Delta G)/dC_{ufw}$ as function of the distance $X$ (in Å) from the silica surface.

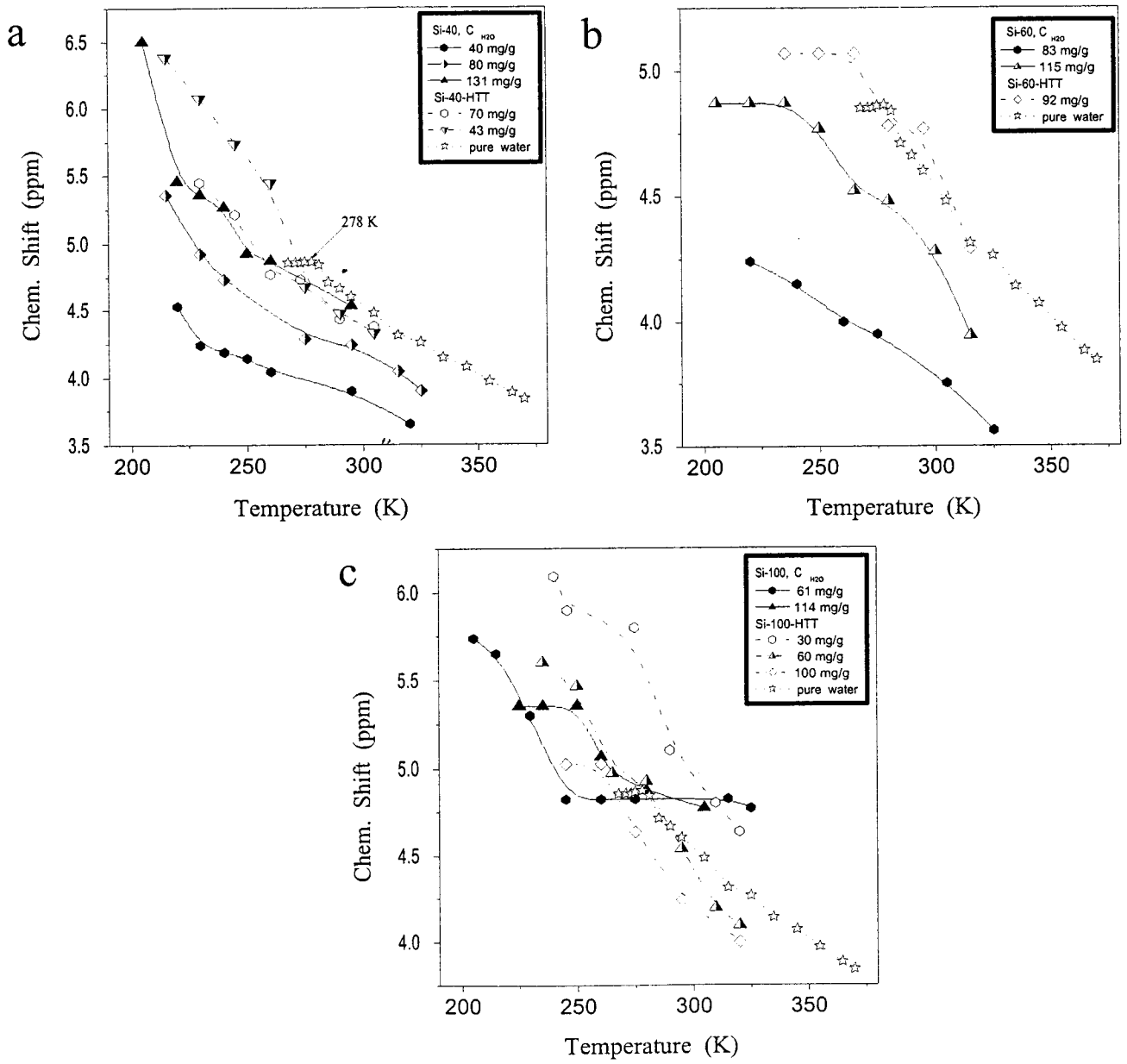


**Figure 14.** Chemical shift of $^1$H in the NMR spectra of water adsorbed from the gas phase as a function of the temperature at different water concentrations on initial and hydrothermally (200 °C) treated Si-40 (a), Si-60 (b), and Si-100 (c); $\delta_H(T)$ is shown for pure water.

**Table 2. Parameters of the Bound Water Layer for Aqueous Suspensions of Silica Gels, Initial and after HTT at 200 °C**

| sample | $\Delta G^s$, kJ/mol | $\Delta G^w$, kJ/mol | $C_w^s$, mg/g | $C_w^w$, mg/g | $\gamma_s$, mJ/m$^2$ |
|---|---|---|---|---|---|
| Si-40 | 3.2 | | 570 | | 92 |
| Si-60 | 3.5 | 1.5 | 540 | 210 | 172 |
| Si-100 | 3.25 | 0.8 | 500 | 250 | 87 |
| S-40HTT | 5.0 | 0.7 | 300 | 320 | 281 |
| Si-60HTT | 4.0 | 0.8 | 200 | 250 | 344 |
| Si-100HTT | 4.0 | 0.75 | 180 | 270 | 323 |

samples (Figure 13d), but such a correlation is absent for initial silica gels (Figure 13c). A similar effect is seen for the derivatives $-d(\Delta G)/dC_{ufw}$ versus $X$ (Figure 13e,f). The $-d(\Delta G)/dC_{ufw}$ value is the analogue of the chemical potential for isobaric freezing of water. Maxima of the dependence of $-d(\Delta G)/dC_{ufw}$ on $X$ correspond to the distances from the silica surfaces characterized more stable complexes (clusters) of the interfacial water. The position of these maxima shifts toward larger $X$ with increasing pore size for both initial and HTT silicas (HTT samples, the $X$ values were computed from a model of a flat surface). These effects can be explained by the significant differences in the unfrozen water layers dependent on the pore size. It should be noted that for Si-40, the $-d(\Delta G)/dC_{ufw}$ maximum corresponds to a water monolayer, but for Si-60 and Si-40HTT, this is three to four monolayers, and for Si-60-HTT and Si-100-HTT, it is five to six water monolayers (Figure 13).

The $\delta_H(T)$ functions (Figure 14) were determined at the adsorbed water concentrations of 30−130 mg per gram of silica gels. These dependences do not have a simple shape in comparison with that for pure water (however, the last has a maximum at approximately 4.5 °C when the water density is maximal; i.e., the hydrogen bond lengths are minimal resulting in larger $\delta_H$[22]) and differ significantly for initial and HTT samples. An incline for some portions of the $\delta_H(T)$ plots is larger or smaller than that for pure water; i.e., the structure of the hydrogen bond network in the interfacial water undergoes significant changes (de-

pending on the sample origin) due to interaction with the silica surfaces. The number of hydrogen bonds per adsorbed molecule is less for Si-40, Si-40-HTT, and Si-60 than that for pure water, Si-60-HTT, and Si-100. However, for Si-100-HTT, there are features in the $\delta_H(T)$ shape dependent on $C_{H_2O}$ (Figure 14c) (or $C_{ufw}$ at $T < 273$ K, however, the $C_{H_2O}$ values were chosen on the $\delta_H(T)$ measurements to provide $C_{ufw} \approx C_{H_2O}$ over nearly the total temperature range). The $\delta_H$ value for a water molecule alone in $CDCl_3$ is $\delta_{H,0} \approx 1.7$ ppm, and for a molecule with four hydrogen bonds in ice, $\delta_{H,4} \approx 7$ ppm.[31,32] The average number ($m$) of the hydrogen bonds per molecule can be estimated as follows

$$m = \frac{\delta_{H,obs} - \delta_{H,0}}{1.325} \qquad (15)$$

The molecular mobility decreases with lowering temperature, which leads to the enhancement of the lifetime of the hydrogen bonds and a decrease in the intermolecular bond lengths, resulting in an increase in $\delta_H$ and $m$. Horizontal portions of the $\delta_H(T)$ plots can be caused by insignificant changes in the structure of the interfacial water with lowering temperature, e.g., in the $m$ values.

## Conclusion

Pyrocarbon forms relatively large globules on the external surfaces of silica gel particles and covers the oxide surfaces by tiny graphene particles. The largest structural changes are observed for adsorbents hydrothermally treated at 200 °C.

The availability of oxygen atoms in pyrolyzed precursors (glucose, acetylacetone) has a substantial influence on the structural parameters of carbosils (both pyrocarbon and silica) in comparison with those for carbosils prepared by acenaphthene carbonization. The temperature of hydrothermal treatment and the origin of pyrocarbon impact the pore structure, and the carbon deposit shielding results in smaller reduction of the specific surface area on such a treatment. Appearance of pyrocarbon on silica gel surfaces influences the nitrogen adsorption energy distributions mainly over the 9−15 kJ/mol range linked with adsorption in relatively narrow mesopores or broad micropores, which markedly change during pyrolysis of organics or subsequent hydrothermal or thermal treatments.

$^1$H NMR investigations with freezing-out of the bulk water in the aqueous suspensions of the initial and hydrothermally treated Si-60, Si-40, and Si-100 demonstrated changes in the structure of the interfacial water for HTT samples appearing in the corresponding dependences of the Gibbs free energy and chemical $^1$H shifts on adsorbed water concentration, temperature, and the sample origin.

**Acknowledgment.** This research was supported by NATO (Grant EST.CLG.976890) and the Polish State Committee for Scientific Research and Ministry of High Education and Science of Ukraine (Grant 2M/303-99). V.M.G. thanks Dr. S. W. Provencher for the CONTIN program package.

LA001094T

(31) Gordon, A. J.; Ford, R. A. *The Chemist's Companion;* Wiley: New York, 1972.

(32) Kinney, D. R.; Chuang, I. S.; Maciel, G. E. *J. Am. Chem. Soc.* **1993,** *115*, 6786.